

Stripe and Bubble Ratchets on Asymmetric Substrates

C. Reichhardt and C. J. O. Reichhardt

*Theoretical Division and Center for Nonlinear Studies,
Los Alamos National Laboratory, Los Alamos, New Mexico 87545, USA*

We show that a variety of non-monotonic ratchet effects can arise when mesophase pattern-forming systems, which exhibit anisotropic crystal, stripe, and bubble regimes, are coupled to one-dimensional asymmetric substrates under ac driving. The ratchet efficiency and direction of motion are determined by how well the mesophase morphology matches the periodicity and shape of the substrate. Stripe states that are aligned with the substrate show the strongest ratchet effect, large bubbles show a weak ratchet effect, and small bubbles show a strong ratchet effect with an efficiency that oscillates as a function of ac drive amplitude. We map out the different rectification phases as a function of the pattern morphology, substrate strength, and ac drive amplitude. The pronounced ratchet effects that we observe in some regimes can be exploited for pattern sorting in hard and soft matter systems.

Introduction— In a rocking ratchet, ac driving produces a net dc drift of particles that are coupled to an underlying asymmetric substrate^{1–3}. Ratchet effects can also occur for Brownian particles moving over asymmetric substrates that flash on and off cyclically^{4,5}. Such effects have been studied extensively in a wide range of particle-like systems, including soft matter^{5,6}, biological systems⁷, and active matter⁸. Ratchet effects also arise in numerous hard condensed matter systems such as vortices in type-II superconductors^{9,10}, magnetic domain walls¹¹, skyrmions¹², Wigner crystals¹³, cold atoms^{14,15}, and quantum systems^{16,17}.

Most studies of ratchet effects have focused on point-like particles or particles that interact via excluded volume; however, there is a broad class of systems that form mesophase or patterned states with higher-order structure such as stripes, labyrinths, void lattices, and bubbles^{18–22}. This type of pattern formation can occur when the particle-particle interaction potential contains multiple length scales^{23–25} or when there is a competition between short range attractive and longer range repulsive interactions^{20,21,26–32}. Mesophases appear in soft matter systems for certain types of colloidal particles, emulsions, binary fluids, and block-copolymer systems, as well as in hard matter systems where bubble and stripe phases are observed for two-dimensional electrons in magnetic fields^{33–37}, certain types of superconducting vortex states^{38–43}, charge ordering systems^{44,45}, and magnetic textures such as stripes and skyrmion bubbles⁴⁶.

If a mesoscale pattern forming state is coupled to a periodic asymmetric substrate and subjected to ac driving, it should be possible to realize a ratchet effect. It has not previously been explored whether ratchet effects occur in such systems or, if so, what type of ratchet effects are present. New ratchet phenomena could arise when the periodicity or morphology of the pattern matches the substrate periodicity. There have been studies of Leidenfrost bubbles coupled to asymmetric substrates where the bubble widths can span the widths of several substrate minima^{47,48}, but the mechanism for the motion is very different from that in particle based systems under ac

driving.

In this work, we consider an assembly of particles that have competing long-range repulsion and short-range attraction where we vary the relative strength of the short range attraction. This model has previously been shown to support a variety of pattern forming states, including anisotropic crystals, stripes, and bubbles^{21,26,29,32}. When the pattern forming states are coupled to an asymmetric substrate and subjected to ac driving, we find a strongly non-monotonic ratchet behavior that depends on the morphology of the pattern. The stripe or highly anisotropic crystalline states can align with the quasi-one-dimensional substrate and generally exhibit a pronounced ratchet effect. Just above the stripe-to-bubble transition, the bubbles are wider than the substrate spacing, can easily distort, and can break up during an ac driving cycle, and in this regime, the ratchet effect is heavily reduced or absent. Small bubbles undergo a strong ratchet effect when the bubble diameter is smaller than the substrate lattice constant and the bubbles are stiff enough to remain intact across the entire ac driving cycle. The behavior of very small bubbles is identical to that of a single particle on an asymmetric substrate, and shows an oscillating ratchet efficiency as a function of ac drive amplitude. We demonstrate that reversals in the direction of ratcheting motion can occur as a function of system density, and show that the ratchet effects are robust over a range of interactions, ac drive amplitudes, and particle densities. The ratchet effect we observe could be used to detect different patterns or as a method for pattern sorting.

Simulation— We consider a two-dimensional system of size $L \times L$ with $L = 36$ that contains N particles with a pairwise interaction potential that has a competition between long range repulsion and short-range attraction,

$$V(R_{ij}) = \frac{1}{R_{ij}} - B \exp(-\kappa R_{ij}) . \quad (1)$$

The distance between particle i and j is $R_{ij} = |\mathbf{R}_i - \mathbf{R}_j|$, and the first term on the right hand side is the long-range repulsive Coulomb term, which favors formation of a uniform triangular lattice. The second term is a

short-range attraction that favors clump formation. The strength and range of the attractive term is controlled by the values of B and κ , and here we fix $\kappa = 1.0$ and vary B . At small R_{ij} , the repulsive term dominates, so complete collapse of the particles onto a point does not occur. The overall potential is repulsive at long length scales, attractive at intermediate scales, and repulsive again at short length scales. In the absence of substrate, as B increases, the system passes through a series of states consisting of uniform crystal, anisotropic crystal, stripes, large bubbles, and small bubbles^{21,26,29,49}. The particle density is given by $\rho = N/L^2$. Recently, this interaction potential was used to study dc depinning on a symmetric one-dimensional substrate, where it was shown that the stripes are strongly pinned and the bubbles have a non-monotonic depinning threshold⁴⁶.

The dynamics of particle i in a sample with periodic boundary conditions in the x and y -directions is obtained using the following overdamped equation:

$$\eta \frac{d\mathbf{R}_i}{dt} = - \sum_{j \neq i}^N \nabla V(R_{ij}) + \mathbf{F}_i^s + \mathbf{F}_{AC}, \quad (2)$$

where the damping term η is set to $\eta = 1.0$. The first term on the right is the particle-particle interaction force, the second term is the substrate force $\mathbf{F}_i^s = \nabla U(x_i)$, and \mathbf{F}_{AC} is the ac driving force. The substrate potential has the form

$$U(x_i) = -U_p [\sin(2\pi x_i/a) + 0.25 \sin(4\pi x_i/a)], \quad (3)$$

where x_i is the x coordinate of particle i and a is the substrate lattice constant. This potential has been used previously to study ratchet effects in soft and hard matter systems^{3,9,12,13}. We characterize the substrate strength by $A_p = U_p/2\pi$, so that the maximum pinning force in the hard or $-x$ direction is $F_p^{\text{hard}} = 1.5A_p$ and in the easy or $+x$ direction is $F_p^{\text{easy}} = 0.725A_p$. The ac driving force has the form $\mathbf{F}_{AC} = F_{AC} \sin(\omega t)$, where we fix $\omega = 0.19$. For each set of parameters, we wait 10^5 simulation time steps after starting the simulation to avoid any transient effects, and then measure the particle velocity in the direction of the drive averaged over 100 ac drive cycles, $\langle V \rangle = \sum_i^N \mathbf{v}_i \cdot \hat{\mathbf{x}}$.

Results— In Fig. 1 we show images of the particle configurations under zero drive, $F_{AC} = 0$, in a system with a substrate strength of $A_p = 1.6$, a particle density of $\rho = 0.44$, and a substrate lattice spacing of $a = 4.5$. Figure 1(a) shows the configuration at $B = 0.0$ where the particle-particle interactions are purely repulsive and an anisotropic crystal appears due to the influence of the substrate. At $B = 2.2$ in Fig. 1(b), we find an aligned stripe state with two rows of particles per substrate minimum. In the bubble state at $B = 2.6$ shown in Fig. 1(c), the bubbles exhibit an asymmetric distortion due to the substrate. For $B = 4.4$ in Fig. 1(d), the bubbles are much smaller and have a circular shape. For this choice of A_p and ρ , the system forms an anisotropic crystal for

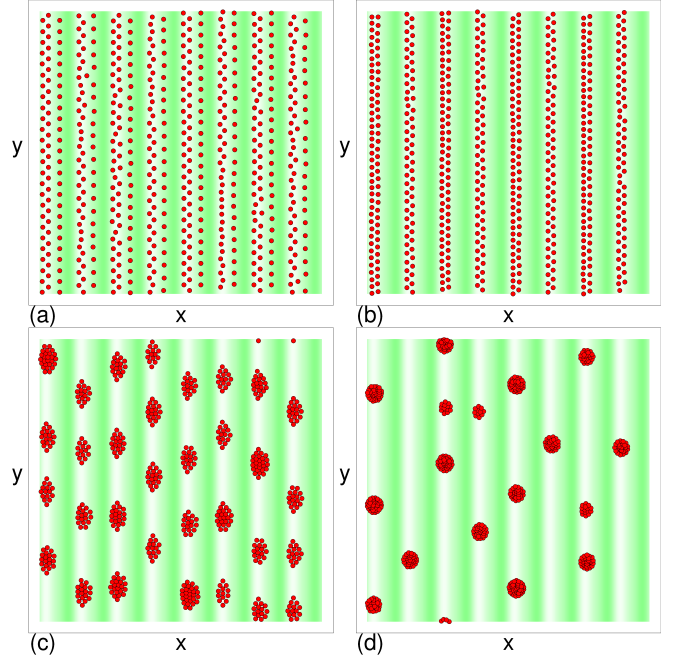


FIG. 1. Image of particle positions (red) and the underlying asymmetric potential (green shading) for samples with substrate strength $A_p = 1.6$, substrate lattice constant $a = 4.5$, and particle density $\rho = 0.44$ under zero driving, $F_{AC} = 0$. (a) $B = 0.0$, where the interaction potential is purely repulsive and the system forms an anisotropic crystal. (b) An aligned stripe state at $B = 2.2$. (c) Disordered large bubbles at $B = 2.6$. (d) Small circular bubbles at $B = 4.4$.

$B < 1.8$, a stripe state for $1.8 \leq B \leq 2.4$, and bubbles for $B > 2.4$.

We next consider the effect of applying an ac drive. In Fig. 2(a) we plot a time series of the instantaneous particle velocity $V(t)$ versus ac cycle number n for the system from Fig. 1 under different combinations of B and F_{AC} . When $F_{AC} = 1.6$, at $B = 0.0$ the response in the $+x$ and $-x$ directions is mostly symmetric, while at $B = 2.2$ in the stripe state, the velocity is strongly asymmetric, indicating the presence of a ratchet effect. When F_{AC} is reduced to $F_{AC} = 0.5$ for $B = 2.2$, the response is symmetric again and the particles simply oscillate within the substrate minima. Figure 2(b) shows $V(t)$ curves obtained in the bubble state. When $F_{AC} = 1.6$, at $B = 2.8$ the response is largely symmetric so the ratchet effect is minimized, while at $B = 4.4$, the response is more asymmetric since there are two velocity peaks in the $+x$ direction for every individual velocity peak in the $-x$ direction, resulting in an enhanced ratchet effect. For $F_{AC} = 0.5$ and $B = 4.4$, the system is pinned. These results indicate that the ratchet response in the bubble state is affected by the size of the bubbles.

To further illustrate the differences in the ratchet behaviors, in Fig. 2(c) we plot the scaled average velocity $2\pi \langle V \rangle / a\omega$ versus F_{AC} in a system with $A_p = 1.0$. Here,

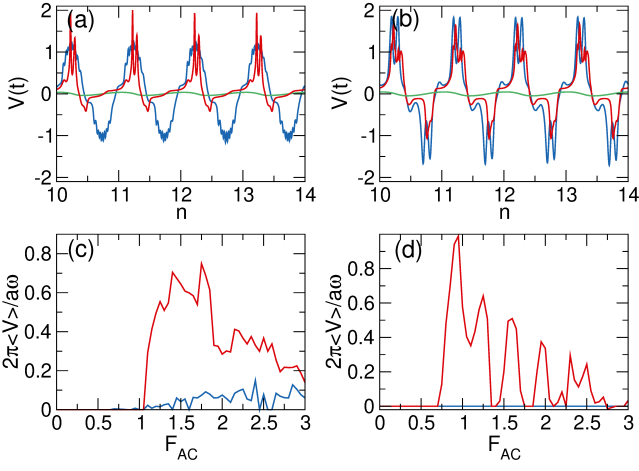


FIG. 2. (a) The instantaneous velocity $V(t)$ vs time in number of ac drive cycles n for the system in Fig. 1 with $A_p = 1.6$, $a = 4.5$, and $\rho = 0.44$ for different combinations of B and F_{AC} . Blue: $B = 0.0$ and $F_{AC} = 1.6$. Red: $B = 2.2$ and $F_{AC} = 1.6$. Green: $B = 2.2$ and $F_{AC} = 0.6$. (b) The same as in (a). Blue: $B = 2.8$ and $F_{AC} = 1.6$. Red: $B = 4.4$ and $F_{AC} = 1.6$. Green: $B = 4.4$ and $F_{AC} = 0.6$. Animations of some of these states appear in the Supplemental Material⁵⁰. (c) The normalized velocity $2\pi\langle V \rangle / \omega a$ vs F_{AC} for a system with $A_p = 1.0$, $a = 4.5$, and $\rho = 0.44$ at $B = 0.0$ (blue) and $B = 2.2$ (red). (d) The same for $B = 2.8$ (blue) and $B = 4.4$ (red).

a value of $2\pi\langle V \rangle / \omega a = 1.0$ indicates that the particles translate an average of one substrate lattice constant per ac drive cycle. When $B = 0.0$, there is a weak ratchet effect at larger values of F_{AC} , while the stripe state at $B = 2.2$ shows a strong ratchet effect for $F_{AC} > 1.0$. The plots of $2\pi\langle V \rangle / \omega a$ versus F_{AC} in Fig. 2(d) indicate that for $B = 2.8$, there is no ratchet effect at any ac drive amplitude, while at $B = 4.4$, there is a strong ratchet effect as well as an oscillation of the ratchet efficiency as function of F_{AC} . The oscillatory ratchet behavior arises from a resonance effect with the substrate period. At the first peak in $2\pi\langle V \rangle / \omega a$, which falls at $F_{AC} = 0.95$, the bubbles translate by one substrate lattice constant during each ac drive cycle, while the peaks at higher values of F_{AC} correspond to ratchet states in which the bubbles traverse multiple substrate minima during each ac drive cycle but have a net translation of less than one substrate lattice constant. Similar oscillatory ratchet behavior has been observed previously for individual particles ratcheting over asymmetric substrates^{9,12}. Increasing the strength of the collective interactions between the particles washes out the resonances with the substrate.

The non-monotonic efficiency of the ratchet effect as a function of B results from the differing ability of the distinct pattern morphologies to couple to the substrate. For the anisotropic crystals at low B , the repulsive interaction term dominates and the particles try to spread apart as shown in Fig. 1(a), so some of the particles are unable to sit in the substrate minima and the ratchet ef-

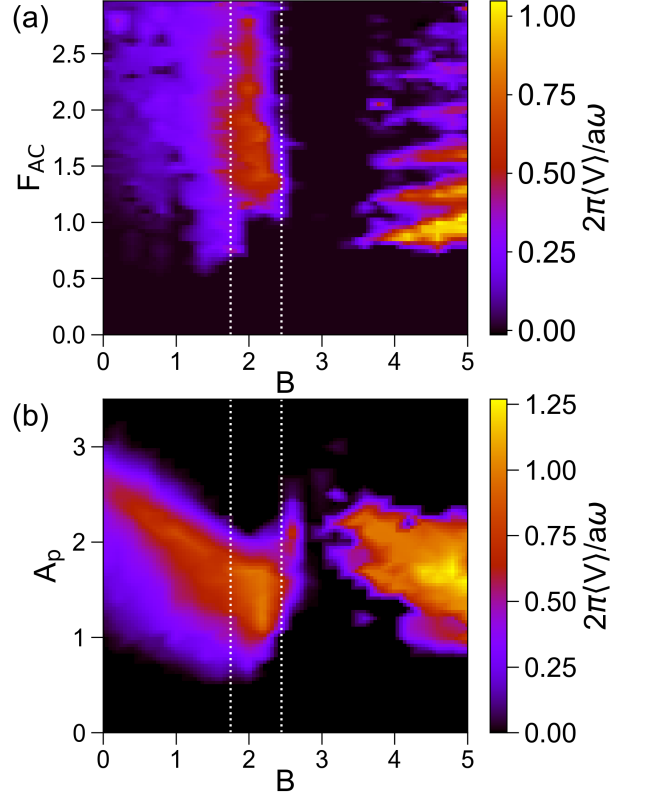


FIG. 3. (a) Heat map of $2\pi\langle V \rangle / \omega a$ as a function of F_{AC} vs B for a system with $A_p = 1.0$. The dashed lines indicate the separation of the stripe state from the lower B anisotropic crystal and the higher B bubble states. (b) The same as a function of A_p vs B for fixed $F_{AC} = 1.6$. In each panel, the ratchet behavior is strongly nonmonotonic and affected by the morphology of the system, with stripes and small bubbles showing the strongest ratchet effect.

fect is reduced. The stripe state illustrated in Fig. 1(b) easily aligns with the substrate, so a majority of the particles can reach the substrate minima and a strong ratchet effect appears. When large bubbles are present, as in Fig. 1(c), a portion of the particles cannot fit inside the substrate minima since the bubble diameter is too wide, which reduces the coupling to the substrate and thereby reduces the magnitude of the ratchet effect; however, the small bubbles that form at higher B fit more easily into the potential minima, as shown in Fig. 1(d), and the ratchet effect becomes large. For very large B , not only are the bubbles smaller but also there are fewer bubbles, so the system approaches the single particle ratchet response limit.

To more clearly demonstrate the nonmonotonic ratchet effect, in Fig. 3(a) we plot a heat map of $2\pi\langle V \rangle / \omega a$ as a function of F_{AC} versus B for a system with $A_p = 1.0$ obtained at F_{AC} and B increments of 0.05 and 0.2, respectively. The dashed lines indicate the separation between the anisotropic crystal state, the stripe state, and

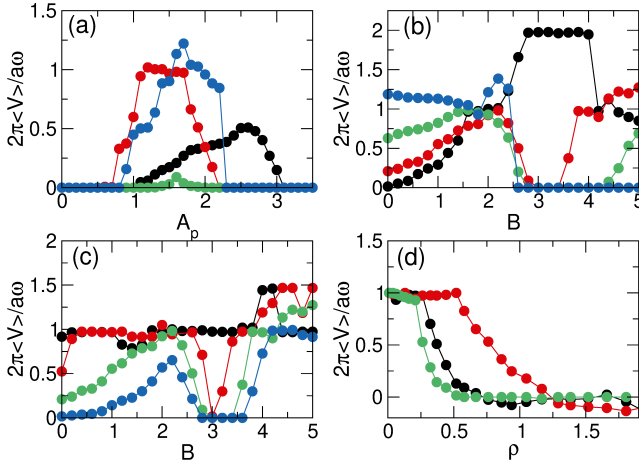


FIG. 4. (a) $2\pi\langle V \rangle / a\omega$ vs A_p for the system in Fig. 3(b) with $\rho = 0.44$, $a = 4.5$, and $F_{AC} = 1.6$ at $B = 0.0$ (black), 2.2 (red), 2.8 (green) and 4.4 (blue). (b) $2\pi\langle V \rangle / a\omega$ vs B for a system with $\rho = 0.44$, $A_p = 1.6$, and $F_{AC} = 1.6$ at different substrate periods $a = 9.0$ (black), 4.5 (red), 3.0 (green), and 2.11 (blue). (c) $2\pi\langle V \rangle / a\omega$ vs B for a system with $a = 4.5$, $A_p = 1.6$, and $F_{AC} = 1.6$ at different densities $\rho = 0.0925$ (black), 0.2083 (red), 0.44 (green), and 0.67 (blue). (d) $2\pi\langle V \rangle / a\omega$ vs ρ for a system with $A_p = 1.6$, $F_{AC} = 1.6$, and $a = 4.5$ at $B = 0.04$ in the anisotropic crystal state (black), $B = 2.2$ in the stripe state (red), and $B = 2.8$ in the large bubble state (green). Images of some of the states appear in the Supplemental Material⁵⁰.

the bubble states. There is a strong ratchet effect for $F_{AC} > 1.0$ in the stripe phase, while the anisotropic crystal shows a reduced ratchet effect. In the large bubble state for $2.4 < B < 3.8$, the ratchet effect is almost completely absent, while for $B > 3.8$, the small bubble state exhibits a strong ratchet effect with oscillatory behavior as a function of F_{AC} . In Fig. 3(b) we show a heat map of $2\pi\langle V \rangle / a\omega$ as a function of A_p vs B at fixed $F_{AC} = 1.6$. There is a strong ratchet effect in the stripe and small bubble regimes and a reduced ratchet effect in the anisotropic crystal and large bubble regimes. For large A_p , the system becomes pinned and the ratchet effect vanishes since each particle is confined to a single substrate minimum, while for $F_p < 0.6$, the ratchet effect also disappears because the system enters a floating phase in which the particles decouple from the substrate. At $B = 0.0$, the separation between particles reaches its greatest extent, and the pinned state does not appear until $A_p > 3.0$.

In Fig. 4(a) we plot $2\pi\langle V \rangle / a\omega$ versus A_p for the system in Fig. 3(b) at $B = 0.0, 2.2, 2.8$, and 4.4 . In the large bubble state at $B = 2.8$, there is only a small region of weak ratcheting motion. To further demonstrate the effects of the morphology on the ratcheting mechanism, in Fig. 4(b) we plot $2\pi\langle V \rangle / a\omega$ versus B in samples with $\rho = 0.44$, $A_p = 1.6$, and $F_{AC} = 1.6$ at different substrate periods of $a = 9.0, 4.5, 3.0$, and 2.11 . For $a = 9.0$, a strong ratchet effect appears for $2.4 < B < 4.0$

since the large bubbles can easily fit inside the substrate troughs due to the large spacing between adjacent substrate minima, and are able to travel a net distance of $2a$ per ac drive cycle. In contrast, when $a = 2.11$ there is no ratchet effect for $B > 2.4$ because the bubble widths are much larger than the substrate spacing. The $a = 3.0$ and $a = 4.5$ curves are similar to each other and show that stripes and small bubbles ratchet while large bubbles do not; however, for $a = 3.0$, the minimum value of B for which the small bubbles begin to ratchet shifts upward.

In Fig. 4(c) we show the $a = 4.5$ system from Fig. 4(b) at varied $\rho = 0.0925, 0.2083, 0.44$, and 0.67 . For $\rho = 0.0925$, the total number of particles in the system is relatively small, so only small anisotropic bubbles form over the entire range of B considered, and there is little variation in the ratchet effect. When $\rho = 0.2083$, the system forms anisotropic bubbles, and there is a dip in the ratchet effect in the large bubble window that appears at $B = 3.0$. For $\rho = 0.44$ and $\rho = 0.67$, there is a reduced ratchet effect in the anisotropic crystal phase, a peak in the ratcheting motion in the stripe phase, an absence of ratcheting in the large bubble state, and a return to ratcheting motion in the small bubble regime. In Fig. 4(d) we plot $2\pi\langle V \rangle / a\omega$ versus ρ for systems with $A_p = 1.6$, $F_{AC} = 1.6$, and $a = 4.5$ at $B = 0.04$ in the anisotropic crystal regime, $B = 2.2$ in the stripe regime, and $B = 2.8$ in the large bubble regime. For $B = 2.8$, a ratchet effect can occur for $\rho < 0.25$ when the bubbles become small enough, due to the reduced number of particles in the system, to fit inside individual substrate minima, but for larger ρ there is no ratchet effect. When $B = 2.2$, a strong ratchet effect occurs for $\rho < 1.23$ and there are weak reversals of the ratchet motion for $\rho > 1.2$. For $B = 0.4$, a strong ratchet effect occurs when $\rho < 0.325$, and there is also a small ratchet reversal for $\rho > 0.73$.

Summary— We have examined the mesophase or pattern forming systems that exhibit crystals, stripes, and various bubble states due to a competition between short-range attraction and long-range repulsion. When we couple these patterns to a quasi-one-dimensional asymmetric substrate and apply ac driving, we find ratcheting motion with strongly nonmonotonic efficiency as a function of the mesophase morphology. The nonmonotonicity is a result of how well or poorly the various mesophases match with the dimensions of the underlying substrate potential. The stripes, which can align with the substrate, show the strongest ratchet effect. Anisotropic crystals show a weaker ratchet effect, and for the large bubbles, ratcheting motion is absent when the diameter of the bubble is larger than the substrate lattice constant. In contrast, small bubbles show a strong ratchet effect because they can fit easily inside individual substrate minima. We show that these effects are robust over a wide range of ac driving amplitudes, substrate strengths, and short-range attraction strength. Our results have implications for a broad array of systems since similar mesophases appear in a wide variety of soft and

hard matter systems, and numerous methods are available to create modulated substrates and apply ac driving to such systems. Since the different morphologies show different ratchet effectiveness, our results could be used to design protocols for sorting patterns in mesophase-forming systems.

ACKNOWLEDGMENTS

We gratefully acknowledge the support of the U.S. Department of Energy through the LANL/LDRD program for this work. This work was supported by the US Department of Energy through the Los Alamos National Laboratory. Los Alamos National Laboratory is operated by Triad National Security, LLC, for the National Nuclear Security Administration of the U. S. Department of Energy (Contract No. 89233321NCA000001).

- ¹ M. O. Magnasco, “Forced thermal ratchets,” *Phys. Rev. Lett.* **71**, 1477–1481 (1993).
- ² L. P. Fauchaux, L. S. Bourdieu, P. D. Kaplan, and A. J. Libchaber, “Optical thermal ratchet,” *Phys. Rev. Lett.* **74**, 1504–1507 (1995).
- ³ P. Reimann, “Brownian motors: noisy transport far from equilibrium,” *Phys. Rep.* **361**, 57–265 (2002).
- ⁴ R. D. Astumian and M. Bier, “Fluctuation driven ratchets: Molecular motors,” *Phys. Rev. Lett.* **72**, 1766–1769 (1994).
- ⁵ J. Rousselet, L. Salome, A. Ajdari, and J. Prost, “Directional motion of Brownian particles induced by a periodic asymmetric potential,” *Nature (London)* **370**, 446–448 (1994).
- ⁶ C. Marquet, A. Buguin, L. Talini, and P. Silberzan, “Rectified motion of colloids in asymmetrically structured channels,” *Phys. Rev. Lett.* **88**, 168301 (2002).
- ⁷ B. Lau, O. Kedem, J. Schwabacher, D. Kwasnieski, and E. A. Weiss, “An introduction to ratchets in chemistry and biology,” *Mater. Horiz.* **3**, 310–318 (2017).
- ⁸ C. J. Olson Reichhardt and C. Reichhardt, “Ratchet effects in active matter systems,” *Ann. Rev. Condens. Matter Phys.* **8**, 51–75 (2017).
- ⁹ C. S. Lee, B. Jankó, I. Derényi, and A. L. Barabási, “Reducing vortex density in superconductors using the ‘ratchet effect’,” *Nature (London)* **400**, 337–340 (1999).
- ¹⁰ Q. Lu, C. J. Olson Reichhardt, and C. Reichhardt, “Reversible vortex ratchet effects and ordering in superconductors with simple asymmetric potential arrays,” *Phys. Rev. B* **75**, 054502 (2007).
- ¹¹ J. H. Franken, H. J. M. Swagten, and B. Koopmans, “Shift registers based on magnetic domain wall ratchets with perpendicular anisotropy,” *Nature Nanotechnol.* **7**, 499–503 (2012).
- ¹² C. Reichhardt, D. Ray, and C. J. Olson Reichhardt, “Magnus-induced ratchet effects for skyrmions interacting with asymmetric substrates,” *New J. Phys.* **17**, 073034 (2015).
- ¹³ C. Reichhardt and C. J. O. Reichhardt, “Collective dynamics and defect generation for Wigner crystal ratchets,” *Phys. Rev. B* **108**, 155131 (2023).
- ¹⁴ C. Mennerat-Robilliard, D. Lucas, S. Guibal, J. Tabosa, C. Jurczak, J.-Y. Courtois, and G. Grynberg, “Ratchet for cold rubidium atoms: The asymmetric optical lattice,” *Phys. Rev. Lett.* **82**, 851–854 (1999).
- ¹⁵ T. Salger, S. Kling, T. Hecking, C. Geckeler, L. Morales-Molina, and M. Weitz, “Directed transport of atoms in a Hamiltonian quantum ratchet,” *Science* **326**, 1241–1243 (2009).
- ¹⁶ H. Linke, T. E. Humphrey, A. Lofgren, A. O. Sushkov, R. Newbury, R. P. Taylor, and P. Omling, “Experimental tunneling ratchets,” *Science* **286**, 2314–2317 (1999).
- ¹⁷ C. Grossert, M. Leder, S. Denisov, P. Hänggi, and M. Weitz, “Experimental control of transport resonances in a coherent quantum rocking ratchet,” *Nature Commun.* **7**, 10440 (2016).
- ¹⁸ M. Seul and D. Andelman, “Domain shapes and patterns - the phenomenology of modulated phases,” *Science* **267**, 476–483 (1995).
- ¹⁹ C. Harrison, D. H. Adamson, Z. Cheng, J. M. Sebastian, S. Sethuraman, D. A. Huse, R. A. Register, and P. M. Chaikin, “Mechanisms of ordering in striped patterns,” *Science* **290**, 1558–1560 (2000).
- ²⁰ A. D. Stoycheva and S. J. Singer, “Stripe melting in a two-dimensional system with competing interactions,” *Phys. Rev. Lett.* **84**, 4657–4660 (2000).
- ²¹ K. Nelissen, B. Partoens, and F. M. Peeters, “Bubble, stripe, and ring phases in a two-dimensional cluster with competing interactions,” *Phys. Rev. E* **71**, 066204 (2005).
- ²² A. Imperio and L. Reatto, “Microphase separation in two-dimensional systems with competing interactions,” *J. Chem. Phys.* **124**, 164712 (2006).
- ²³ G. Malescio and G. Pellicane, “Stripe phases from isotropic repulsive interactions,” *Nature Mater.* **2**, 97–100 (2003).
- ²⁴ M. A. Glaser, G. M. Grason, R. D. Kamien, A. Kosmrlj, C. D. Santangelo, and P. Ziherl, “Soft spheres make more mesophases,” *EPL* **78**, 46004 (2007).
- ²⁵ E. Edlund and M. N. Jacobi, “Universality of striped morphologies,” *Phys. Rev. Lett.* **105**, 137203 (2010).
- ²⁶ C. Reichhardt, C. J. Olson Reichhardt, I. Martin, and A. R. Bishop, “Dynamical ordering of driven stripe phases in quenched disorder,” *Phys. Rev. Lett.* **90**, 026401 (2003).
- ²⁷ F. Sciortino, S. Mossa, E. Zaccarelli, and P. Tartaglia, “Equilibrium cluster phases and low-density arrested disordered states: The role of short-range attraction and long-range repulsion,” *Phys. Rev. Lett.* **93**, 055701 (2004).
- ²⁸ Y. H. Liu, L. Y. Chew, and M. Y. Yu, “Self-assembly of complex structures in a two-dimensional system with competing interaction forces,” *Phys. Rev. E* **78**, 066405 (2008).
- ²⁹ C. J. Olson Reichhardt, C. Reichhardt, and A. R. Bishop, “Structural transitions, melting, and intermediate phases for stripe- and clump-forming systems,” *Phys. Rev. E* **82**, 041502 (2010).
- ³⁰ J.-X. Chen, J.-W. Mao, S. Thakur, J.-R. Xu, and F. Liu, “Dynamical phase of driven colloidal systems with short-range attraction and long-range repulsion,” *J. Chem. Phys.*

- 135**, 094504 (2011).
- ³¹ D. McDermott, C. J. Olson Reichhardt, and C. Reichhardt, “Stripe systems with competing interactions on quasi-one dimensional periodic substrates,” *Soft Matter* **10**, 6332–6338 (2014).
 - ³² A. Hooshanginejad, J.-W. Barotta, V. Spradlin, G. Pucci, R. Hunt, and D. M. Harris, “Interactions and pattern formation in a macroscopic magnetocapillary salt system of mermaid cereal,” *Nature Commun.* **15**, 5466 (2024).
 - ³³ M. M. Fogler, A. A. Koulakov, and B. I. Shklovskii, “Ground state of a two-dimensional electron liquid in a weak magnetic field,” *Phys. Rev. B* **54**, 1853–1871 (1996).
 - ³⁴ R. Moessner and J. T. Chalker, “Exact results for interacting electrons in high Landau levels,” *Phys. Rev. B* **54**, 5006–5015 (1996).
 - ³⁵ E. Fradkin and S. A. Kivelson, “Liquid-crystal phases of quantum Hall systems,” *Phys. Rev. B* **59**, 8065–8072 (1999).
 - ³⁶ M. P. Lilly, K. B. Cooper, J. P. Eisenstein, L. N. Pfeiffer, and K. W. West, “Anisotropic states of two-dimensional electron systems in high Landau levels: Effect of an in-plane magnetic field,” *Phys. Rev. Lett.* **83**, 824–827 (1999).
 - ³⁷ J. Göres, G. Gamez, J. H. Smet, L. Pfeiffer, K. West, A. Yacoby, V. Umansky, and K. von Klitzing, “Current-induced anisotropy and reordering of the electron liquid-crystal phases in a two-dimensional electron system,” *Phys. Rev. Lett.* **99**, 246402 (2007).
 - ³⁸ E. Babaev and M. Speight, “Semi-Meissner state and neither type-I nor type-II superconductivity in multicomponent superconductors,” *Phys. Rev. B* **72**, 180502 (2005).
 - ³⁹ X. B. Xu, H. Fangohr, S. Y. Ding, F. Zhou, X. N. Xu, Z. H. Wang, M. Gu, D. Q. Shi, and S. X. Dou, “Phase diagram of vortex matter of type-II superconductors,” *Phys. Rev. B* **83**, 014501 (2011).
 - ⁴⁰ S.-Z. Lin and X. Hu, “Vortex states and the phase diagram of a multiple-component Ginzburg-Landau theory with competing repulsive and attractive vortex interactions,” *Phys. Rev. B* **84**, 214505 (2011).
 - ⁴¹ H. J. Zhao, V. R. Misko, and F. M. Peeters, “Analysis of pattern formation in systems with competing range interactions,” *New J. Phys.* **14**, 063032 (2012).
 - ⁴² K. A. H. Sellin and E. Babaev, “Stripe, gossamer, and glassy phases in systems with strong nonpairwise interactions,” *Phys. Rev. E* **88**, 042305 (2013).
 - ⁴³ Q. Meng, C. N. Varney, H. Fangohr, and E. Babaev, “Phase diagrams of vortex matter with multi-scale inter-vortex interactions in layered superconductors,” *J. Phys.: Condens. Matter* **29**, 035602 (2017).
 - ⁴⁴ V. J. Emery, S. A. Kivelson, and J. M. Tranquada, “Stripe phases in high-temperature superconductors,” *Proc. Natl. Acad. Sci. (USA)* **96**, 8814–8817 (1999).
 - ⁴⁵ B. P. Stojković, Z. G. Yu, A. L. Chernyshev, A. R. Bishop, A. H. Castro Neto, and N. Grønbech-Jensen, “Charge ordering and long-range interactions in layered transition metal oxides: A quasiclassical continuum study,” *Phys. Rev. B* **62**, 4353–4369 (2000).
 - ⁴⁶ C. Reichhardt and C. J. O. Reichhardt, “Peak effect and dynamics of stripe- and pattern-forming systems on a periodic one-dimensional substrate,” *Phys. Rev. E* **109**, 054606 (2024).
 - ⁴⁷ H. Linke, B. J. Alemán, L. D. Melling, M. J. Taormina, M. J. Francis, C. C. Dow-Hygelund, V. Narayanan, R. P. Taylor, and A. Stout, “Self-propelled Leidenfrost droplets,” *Phys. Rev. Lett.* **96**, 154502 (2006).
 - ⁴⁸ G. Lagubeau, M. Le Merrer, C. Clanet, and D. Quéré, “Leidenfrost on a ratchet,” *Nature Phys.* **7**, 395–398 (2011).
 - ⁴⁹ X. B. Xu, T. Tang, Z. H. Wang, X. N. Xu, G. Y. Fang, and M. Gu, “Nonequilibrium pattern formation in circularly confined two-dimensional systems with competing interactions,” *Phys. Rev. E* **103**, 012604 (2021).
 - ⁵⁰ See Supplemental Material for supplementary figures and videos.

Supplemental information for “Stripe and Bubble Ratchets on Asymmetric Substrates”

C. Reichhardt and C. J. O. Reichhardt
Theoretical Division, Los Alamos National Laboratory,
Los Alamos, New Mexico 87545 USA

We show additional images of the particle configurations for states with and without strong ratcheting effects. In Fig. S1 we plot images of the stripe state at $B = 2.2$ from Fig. 4(a) of the main text. When $A_p = 0.2$ in Fig. S1(a), the particles float above the substrate and do not couple to it, resulting in the absence of a ratchet effect, while for $A_p = 3.5$ in Fig. S1(b), the particles remain completely pinned by the substrate and there is no ratchet motion.

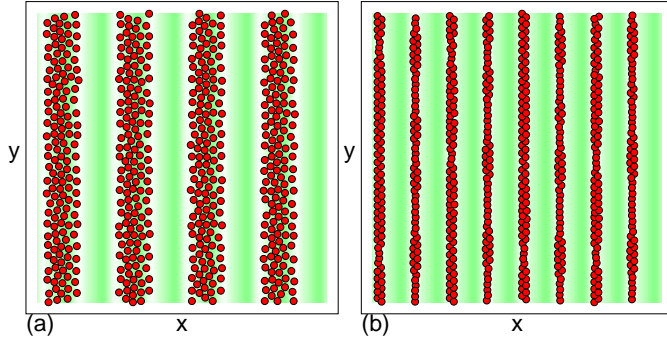


FIG. S1. Image of particle positions (red) and the underlying asymmetric potential (green shading) for samples with $F_{AC} = 1.6$, $a = 4.5$, $\rho = 0.44$, and $B = 2.2$ at (a) $A_p = 0.2$, where there is no ratchet effect and the particles are floating above the substrate, and at (b) $A_p = 3.5$, where the system is pinned.

In Fig. S2(a,b) we plot images of the bubble state from Fig. 4(b) of the main text. At $a = 9.0$ and $B = 2.8$ in Fig. S2(a), the size of the bubbles matches the size of the substrate lattice constant and there is a strong ratchet effect, while at $a = 2.11$ and $B = 2.4$ in Fig. S2(b), the bubbles are too wide to fit fully inside the substrate troughs and there is no ratchet effect. In the anisotropic crystal regime for this sample at $a = 2.11$ and $B = 0.4$, shown in Fig. S2(c), a strong ratchet effect is present.

In Fig. S3 we plot images of the bubble state at $B = 4.4$ from Fig. 4(c) of the main text. For $\rho = 0.0925$ in Fig. S3(a), the small number of particles present in the system produces narrow bubbles that couple well to the substrate and experience a strong ratchet effect. At $\rho = 0.67$ in Fig. S3(b), the bubbles are too wide to fit fully inside the substrate troughs and there is no ratchet effect.

In Fig. S4 we plot images of the from Fig. 4(d) of the

main text. For the stripe state at $B = 4.2$ in Fig. S4(a), there is a forward or $+x$ direction ratchet effect. In the

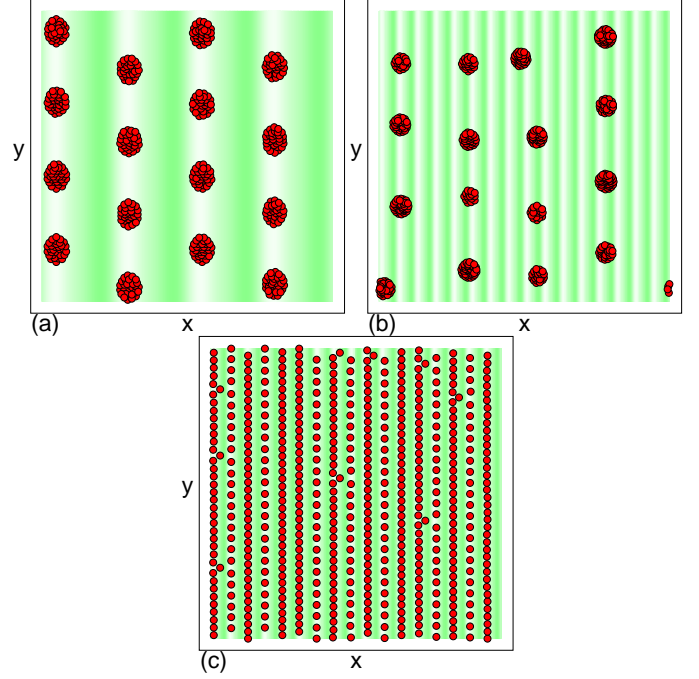


FIG. S2. Image of particle positions (red) and the underlying asymmetric potential (green shading) for samples with $A_p = 1.6$ and $\rho = 0.44$ at (a) $a = 9.0$ and $B = 2.8$, where there is a strong ratchet effect, (b) $a = 2.11$ and $B = 2.4$, where there is no ratchet effect, and (c) $a = 2.11$ and $B = 0.4$, where there is a strong ratchet effect.

bubble state at $B = 4.8$, shown in Fig. S4(b), no ratchet effect appears. Finally, in the anisotropic crystal state at $B = 0.4$ in Fig. S4(c), a weak reverse or $-x$ direction ratchet effect occurs.

Supplemental Movie 1: Motion of the system in Fig. 2(a) of the main text with $A_p = 1.6$, $a = 4.5$, $\rho = 0.44$, and $B = 2.2$ at $F_{AC} = 1.6$, where there is a strong ratchet effect.

Supplemental Movie 2: Motion of the system in Fig. 2(b) of the main text with $A_p = 1.6$, $a = 4.5$, $\rho = 0.44$, and $B = 2.8$ at $F_{AC} = 1.6$, where there is a weak ratchet effect.

Supplemental Movie 3: Motion of the system in Fig. 2(b) of the main text with $A_p = 1.6$, $a = 4.5$, $\rho = 0.44$, and $B = 4.4$ at $F_{AC} = 1.6$, where there is a strong ratchet effect.

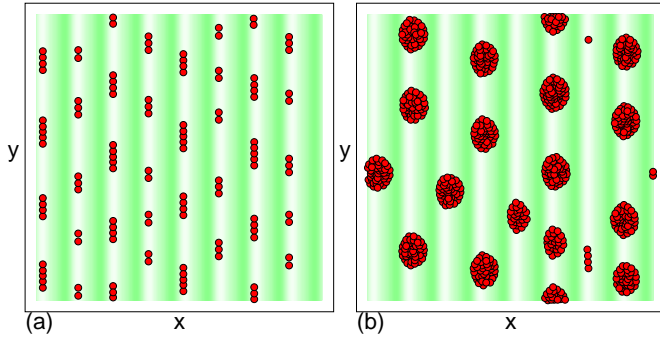


FIG. S3. Image of particle positions (red) and the underlying asymmetric potential (green shading) for samples with $A_p = 1.6$, $a = 4.5$, and $B = 4.4$ at (a) $\rho = 0.0925$, where there is a strong ratchet effect, and (b) $\rho = 0.67$, where there is no ratchet effect.

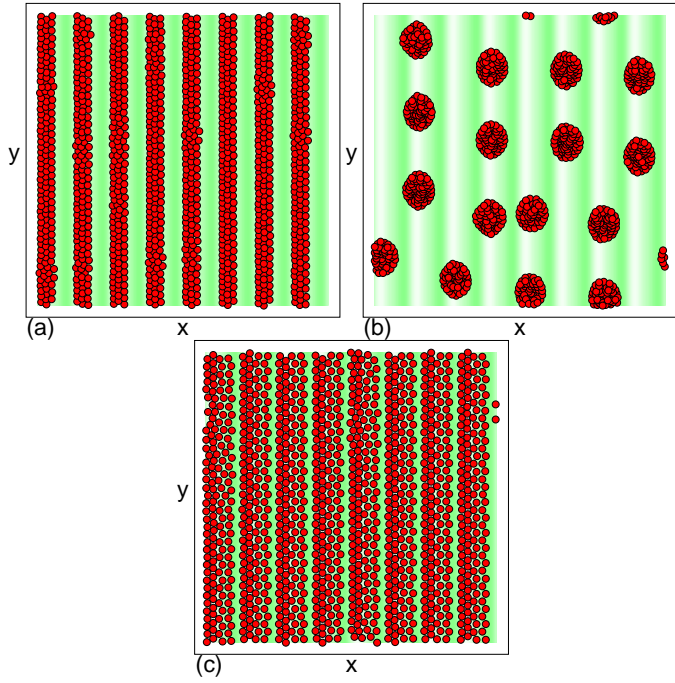


FIG. S4. Image of particle positions (red) and the underlying asymmetric potential (green shading) for samples with $A_p = 1.6$, $a = 4.5$, and $\rho = 0.9382$ at (a) $B = 4.2$, where there is a forward ($+x$ direction) ratchet effect, (b) $B = 4.8$ where there is no ratchet effect, and (c) $B = 0.4$ where there is an anisotropic crystal with a weak reverse ($-x$ direction) ratchet effect.